Hindawi Publishing Corporation
Journal of Nanomaterials
Volume 2011, Article ID 307589, 8 pages
doi:10.1155/2011/307589

Research Article

Preparation, Characterization, and Modeling of Carbon Nanofiber/Epoxy Nanocomposites

Lan-Hui Sun,[1] Zoubeida Ounaies,[2] Xin-Lin Gao,[3] Casey A. Whalen,[2] and Zhen-Guo Yang[1]

[1] *Department of Materials Science, Fudan University, Shanghai 200433, China*
[2] *Department of Aerospace Engineering, Texas A&M University, College Station, TX 77843, USA*
[3] *Department of Mechanical Engineering, Texas A&M University, College Station, TX 77843, USA*

Correspondence should be addressed to Zoubeida Ounaies, zounaies@tamu.edu

Received 6 July 2010; Accepted 19 October 2010

Academic Editor: Sulin Zhang

There is a lack of systematic investigations on both mechanical and electrical properties of carbon nanofiber (CNF)-reinforced epoxy matrix nanocomposites. In this paper, an in-depth study of both static and dynamic mechanical behaviors and electrical properties of CNF/epoxy nanocomposites with various contents of CNFs is provided. A modified Halpin-Tsai equation is used to evaluate the Young's modulus and storage modulus of the nanocomposites. The values of Young's modulus predicted using this method account for the effect of the CNF agglomeration and fit well with those obtained experimentally. The results show that the highest tensile strength is found in the epoxy nanocomposite with a 1.0 wt% CNFs. The alternate-current (AC) electrical properties of the CNF/epoxy nanocomposites exhibit a typical insulator-conductor transition. The conductivity increases by four orders of magnitude with the addition of 0.1 wt% (0.058 vol%) CNFs and by ten orders of magnitude for nanocomposites with CNF volume fractions higher than 1.0 wt% (0.578 vol%). The percolation threshold (i.e., the critical CNF volume fraction) is found to be at 0.057 vol%.

1. Introduction

Carbon nanofibers (CNFs) are electrically and thermally conductive and have very good mechanical properties. Research on carbon nanofiber-reinforced nanocomposites has been mainly focusing on carbon nanotube (CNT)-filled nanocomposites. This is due to the fact that CNTs have fewer microstructural defects than CNFs, resulting in better overall properties as well as smaller dimensions and a lower density. However, CNFs are less expensive and can be manufactured at high yields, justifying further in-depth investigation of their impact on nanocomposites.

CNFs have a cup-stacked structure which results from the vapor deposition process used to produce them [1, 2]. The relatively low efficiency of catalyst results in microstructural defects in CNFs, which require special treatments in order for CNFs to achieve desired properties. A number of treatment methods have been used, which include acid treatment [3, 4], heat treatment (to eliminate defects) [5], plasma treatment (to purify) [6], and surface functionalization (to improve interface adhesion) [7, 8]. Because of their high aspect ratio and high surface energy (due to nanoscale diameters), CNFs tend to agglomerate, leading to inhomogeneous dispersion. Many efforts have been made to deagglomerate CNFs using methods such as diluting the matrix with solvents [6, 9] and combining mechanical mixing with sonication [9, 10].

Good dispersion of CNFs leads to an enhancement in both strength and modulus of nanocomposites [9, 11–14]. Choi et al. [9] found that CNF/epoxy nanocomposites had a maximum tensile strength and a large Young's modulus with 5 wt% CNFs, and a reduced fracture strain with increasing filler content. In addition, both the storage modulus and the glass transition temperature (T_g) increased due to the incorporation of CNFs. A study by Zhou and coworkers [14] indicated that the modulus of CNF/epoxy nanocomposites increased continuously with increasing CNF content, but the tensile strength decreased with further increasing CNF content beyond 2 wt% CNF. DMA studies revealed that with 3 wt% CNFs, there was a 65% enhancement in the storage modulus at room temperature and a 6°C increase

in T_g. Xu et al. [15] demonstrated that there was only very little increase in mechanical properties of CNF/epoxy nanocomposites, ever though they used GCNF-ODA reactive linkers to improve the interface of CNFs and epoxy.

Because of their high electrical conductivity, CNFs have been used as fillers to improve electrical properties of polymeric composites in a number of studies [3, 4, 10, 16–19]. A remarkable increase in electrical conductivity was observed when CNF volume fraction exceeded the percolation threshold. For CNF/epoxy nanocomposites, Allaoui et al. [10] found a percolation threshold at a very low critical CNF weight fraction of 0.064%. The insulator-to-conductor transition region spanned about one order of magnitude of the CNF weight fraction from 0.1 to 1.2%. Far from the transition, the conductivity increased by two orders of magnitude. Other studies on electrical properties of CNF/epoxy nanocomposites did not focus on the percolation behavior, but rather on the effect of CNFs' heat treatment [5] or on the effect of the viscosity of epoxy matrix [9] on the electrical conductivity of CNF/epoxy nanocomposites. Moreover, none of these papers discussed the dielectric properties of CNF/epoxy nanocomposites.

So far, there has been no study that specifically focuses on the simultaneous characterization of mechanical and electrical properties of solvent-processed CNF/epoxy nanocomposites. In addition, the existing results concerning the impact of CNFs on mechanical behavior of epoxy nanocomposites appear to be inconsistent, as reviewed above. This motivated the current study.

In this paper, CNF/epoxy nanocomposites with various contents of CNFs were prepared. Both static and dynamic mechanical properties as well as electrical and dielectric properties of the nanocomposites were investigated, and fracture surfaces were observed in order to better understand the fracture mechanisms. Also, the Young's modulus and storage modulus were predicted using a modified Halpin-Tsai equation, which fitted the experimental results well.

2. Experimental Study

2.1. Preparation of Nanocomposites. Carbon nanofibers (Pyrograf-III) were supplied by Applied Science, Inc. (ASI). The carbon nanofibers have diameters ranging from 100 to 200 nm and lengths from 30 to 100 μm. The acquired carbon nanofibers were heat treated up to 3000°C. A purification process was also utilized to remove the undesirable impurities. The purification process consisted of refluxing the CNFs in dichloromethane—CH_2Cl_2 (Aldrich, Co.) for five days at 35°C, followed by several deionized H_2O washes and second-time refluxing for 24 hours. The nanofibers were rinsed again, vacuum filtered for 24 hours and dried at 110°C for at least 24 hours, and then examined for water content. The purified CNFs were properly stored in closed hygroscopic containers, since retained moisture could prevent proper mixing.

CNF/epoxy nanocomposites with CNF content ranging from 0 to 2 wt% were fabricated. First, a desired amount of CNFs was immersed into Dimethylacetamide (DMAc). The solution was sonicated and mechanically stirred for 1 hour. Epoxy resin (Epon 862, Hexion Specialty Chemicals, Inc.) was then added, and the new solution was sonicated and mechanically stirred for another 3 hours. The solution was then evaporated in an enclosed vacuum at 80°C over night to eliminate all the DMAc. Curing agent (EpiKure W, Hexion Specialty Chemicals, Inc.) was then used, and the new solution was sonicated and mechanically mixed for half an hour. Before casting, the solution was degassed in a vacuum overnight to remove trapped gasses. Finally, the solution was cast into different molds to get samples for mechanical and electrical tests. The samples were heated and cured for 2 hours at 125°C and another 2 hours at 177°C.

2.2. Tensile Tests and SEM. Mechanical properties were measured on an MTS universal testing machine at a constant displacement rate of 0.5 mm/min. The specimen had a width of 13 mm and a thickness of 2.5 mm. The gauge length was 60 mm. The tensile strength and Young's modulus were calculated from the recorded stress levels at the constant displacement rate. All tensile tests were performed at room temperature, and three specimens (or more) were used for each CNF content. The average value for each specimen type was recorded. The tensile stress-strain curves were plotted after calculating the engineering stress and engineering strain.

Fracture surfaces of the tensile specimens were observed using a scanning electron microscope (SEM, JEOL JSM-6400) to study the failure mechanisms and the post-fracture dispersion of CNFs. Before the SEM observations, the specimens were coated with a thin layer of platinum.

2.3. Dynamic Mechanical Analysis. Dynamic mechanical analysis (DMA) was performed on a RSA-III DMA from 25 to 200°C at a temperature scanning rate of 3°C/min. The tests were operated in the three-point bending mode at an oscillation frequency of 1 Hz. The rectangular specimens were 30 mm long, 9 mm, wide and 3 mm thick. Three samples of each CNF content were tested. The glass transition temperature (T_g) was assigned as the temperature where the loss factor was recorded as a maximum.

2.4. Electrical Measurements. Alternate-current (AC) conductivity and dielectric constant of pure epoxy and CNF/epoxy nanocomposites were measured using an impedance analyzer (Novocontrol Alpha Analyzer) in a frequency range of 10^{-2}–10^7 Hz. The specimens were coated with an electrodeposited silver layer (100 nm thick) on the two opposite surfaces to ensure a good electrical contact area between the electrodes and specimen. The samples had a bulk size of 1.5 cm × 1.5 cm. The silver electrode area was circular with a diameter of 0.5 cm. Each measurement shown was an average of 3 to 4 samples. The setup was based on a parallel plate configuration, where the parallel capacitance (C_p) was measured at each frequency and was then converted to dielectric constant $\varepsilon = C_p t/(A\varepsilon_0)$, where t is the thickness of the sample (~0.5 mm), A is the electrode area, and ε_0 is the permittivity of free space (=8.85 × 10^{-12} F/m).

Table 1: Tensile properties of CNF/epoxy nanocomposites.

Sample	Tensile strength (MPa)	Toughness (MJ/m^3)	Young's Modulus (GPa)
Pure Epon862	68.7 ± 2.5	397.6 ± 33.2	1.04 ± 0.04
0.05% CNF	70.9 ± 2.6	418.2 ± 41.9	1.06 ± 0.06
0.1% CNF	71.0 ± 3.7	550.0 ± 23.6	1.09 ± 0.01
0.5% CNF	73.0 ± 1.4	610.2 ± 39.3	1.16 ± 0.01
1% CNF	74.4 ± 2.4	562.7 ± 28.0	1.22 ± 0.01
2% CNF	62.1 ± 2.5	244.5 ± 30.8	1.29 ± 0.02

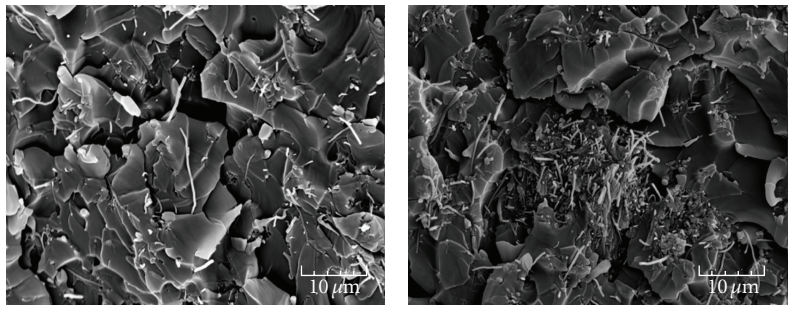

(a) 1 wt% CNFs (b) 2 wt% CNFs

Figure 1: Dispersion of CNFs in epoxy.

3. Results and Discussion

3.1. Tensile Properties. The tensile properties of the CNF/epoxy nanocomposites with the CNF content varying from 0 to 2 wt% are shown in Table 1. It is seen that the tensile strength increases with increasing content of CNFs until 1 wt%, beyond which the tensile strength decreases. Figure 1 shows the dispersion of CNFs in the nanocomposites with 1 wt% and 2 wt% CNFs. For the 1 wt% CNF/epoxy nanocomposite, the CNFs are homogeneously dispersed as individual fibers. However, the CNFs in the 2 wt% CNF/epoxy nanocomposite are agglomerated and clustered as bundles with a diameter of about 10 μm. These bundles act as stress concentration sites, leading to the nonuniform stress distribution and high stresses near the bundles. During the tensile test, the epoxy matrix around these bundles breaks quickly due to the elevated stresses, resulting in the decrease in tensile strength of this nanocomposite.

The area under the stress-strain curve is known as toughness, which represents the total strain energy per unit volume in the material induced by the applied stress. The addition of uniformly dispersed CNFs can significantly increase the toughness of the epoxy, as indicated in Table 1. The toughness increases by 42% with the addition of 1 wt% CNFs and decreases by 39% with the addition of 2 wt% CNFs, both relative to the pure epoxy (Epon 862). To better understand the toughening mechanism of the CNF/epoxy nanocomposites, SEM is used to observe the fracture surfaces.

From the fracture surface of the pure epoxy (Figure 2(a)), it can be seen that large and flat cleavage planes indicate typical characteristic of brittle fracture. For a 0.05 wt% CNF/epoxy nanocomposite (Figure 2(b)), the fracture surface becomes more rough, and the cleavage planes become smaller than those of the pure epoxy. Large cracks propagate along low CNF density areas, leading to ridges. Cleavage planes are evenly distributed and are the smallest for a 1 wt% CNF/epoxy nanocomposite (Figure 2(c)). The increased number of cleavage planes results in more areas capable of absorbing the fracture energy, which leads to a higher crack propagation resistance. An inspection of Figure 1(a) again reveals some fiber pullout, indicating that the fiber-matrix adhesion is not optimal. From these observations, it appears that this nanocomposite has the highest toughness. However, matrix cracks are evident on the fracture surface of the 2 wt% CNF/epoxy nanocomposite (Figure 2(d)). This suggests that a lot of microcracks may have started from the clusters of CNFs. With the increase of the applied load, these microcracks would quickly connect with each other to form macrocracks, leading to fracture of the nanocomposite.

The Halpin-Tsai equation links the modulus of a unidirectional fiber composite to the fiber volume fraction [20, 21]. Many studies have been conducted to predict the modulus of a fiber-reinforced composite with randomly aligned discontinuous fibers by using variants of the Halpin-Tsai equation. In most of these studies, an orientation factor, α, was introduced to account for the random fiber orientation. In [22], the Halpin-Tsai equation was modified to be

$$\frac{E_c}{E_m} = \frac{1 + c\eta v_f}{1 - \eta v_f} \quad \text{with } \eta = \frac{\left(\alpha E_f/E_m\right) - 1}{\left(\alpha E_f/E_m\right) + c}, \tag{1}$$

where E_c, E_m, and E_f are, respectively, the moduli of the composite, matrix, and fiber (carbon nanotubes), v_f is

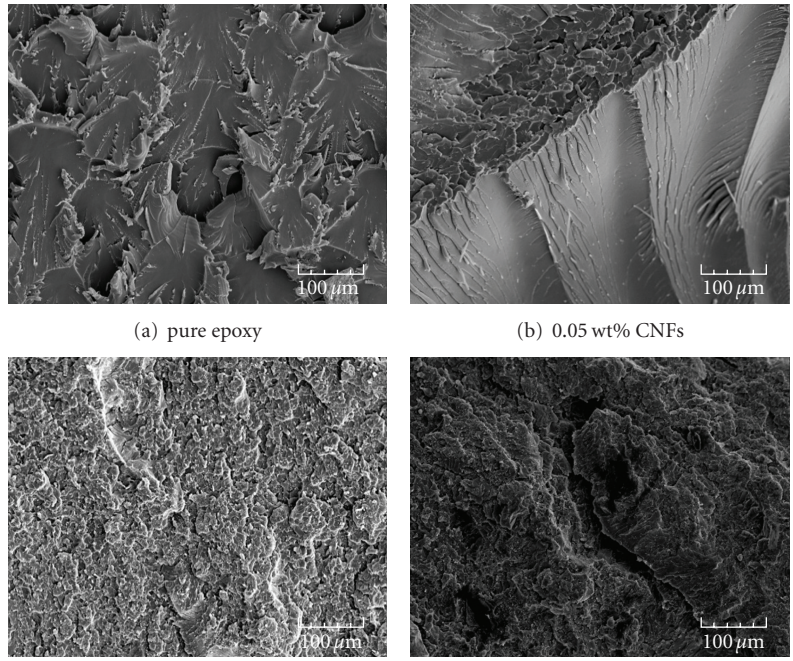

(a) pure epoxy (b) 0.05 wt% CNFs

(c) 1 wt% CNFs (d) 2 wt% CNFs

Figure 2: Fracture surface morphology.

the fiber volume fraction, and $c = 2l/d$ is the shape factor relating to the aspect ratio of the reinforcement length (l) over the diameter (d). They further modified the Halpin-Tsai equation by changing the shape factor c to $\xi = (2l/d)e^{-av_f - b}$, which is an exponential relation, with a and b being constants that are related to the degree of CNF agglomeration.

In this study, the Young's moduli of the epoxy matrix and CNF are 1.04 GPa and 400 GPa, respectively. The orientation factor α is taken to be 0.184 (after [23]). The aspect ratio of the CNFs is about 150. The effects of the constants a and b on the Young's modulus predicted using the modified Halpin-Tsai equation are shown in Figures 3(a) and 3(b). It can be seen that increasing the constant a tends to bend the curves, while increasing the constant b lowers the height of the curves.

By varying the values of a and b, a best fit to the experimentally obtained Young's modulus is found when $a = 120$ and $b = 1$. This best fit is displayed in Figure 3(b), for which $\xi = 300e^{-120v_f - 1}$. Good agreement between the experimental data and predicted results over the range of fiber volume fractions investigated indicates that CNF/epoxy nanocomposites are 3D randomly oriented systems with agglomeration of CNFs at higher volume fractions.

3.2. Dynamic Mechanical Analysis. The effects of CNFs on the storage modulus of the CNF/epoxy nanocomposites are illustrated in Figure 4. The addition of CNFs increases the storage modulus of epoxy at temperatures both below and above the glass transition temperature (T_g). The maximum storage modulus is observed in the nanocomposite with 1 wt% CNFs, which is, respectively, about 18% and 70% higher than that of the pure epoxy below and above the glass transition temperature. The presence of CNFs inhibits the movement of molecular chains around the CNFs. This is due to the high surface energy of CNFs absorbing the motion of the molecular chains around them. Because of this interaction between CNFs and the molecular chains, the force imposed on the CNF/epoxy nanocomposites transfers to the stiff CNFs and leads to the increased storage modulus. The storage modulus starts to decrease at 2 wt% CNF content. This is due to the poor dispersion of CNFs at higher contents, which can be seen from the SEM images in Figure 1.

T_g represents a major transition for many polymers, as physical properties change significantly when the material goes from the glassy state to the rubber-like state. For cured polymers it appears that DMA is 10 to 100 times more sensitive to the changes occurring near T_g than differential scanning calorimetry [24]. T_g is usually determined from the peak of the loss factor ($\tan\delta$) curves. Figure 5 shows the loss factor curves of the pure epoxy and the CNF/epoxy nanocomposites. A small increase in T_g is found at CNF content lower than 2 wt%. CNFs restrict the segmental movement of molecular chains, resulting in a higher T_g. The peak height of the loss factor of the nanocomposites decreases with the increasing content of CNFs. As mentioned in [25], the relative heights in T_g are inversely proportional to the volume fraction of confined segments in the interface layer. On the other hand, with the increasing content of the uniformly dispersed CNFs, more interactions between molecular chains and CNFs occur.

For the nanocomposite with 2 wt% CNFs, there are a decrease in T_g and a broadening of the peak. The decrease in T_g is due to the agglomeration of the CNFs in the

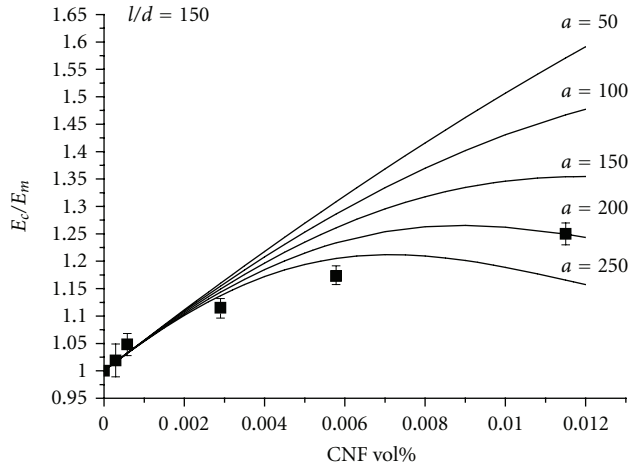

(a) Effect of the constant a

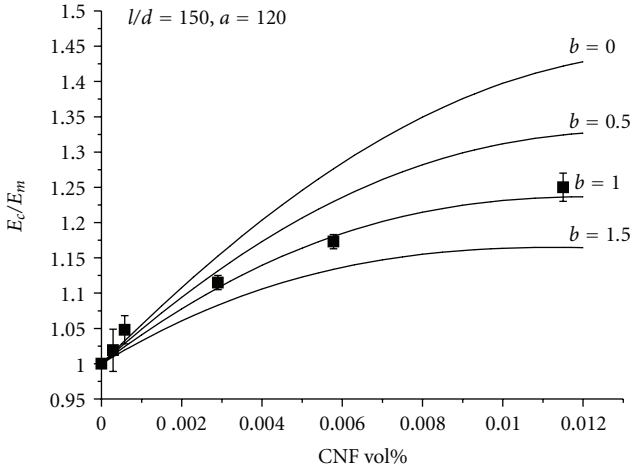

(b) Effect of the constant b

Figure 3: Effects of a and b on the predicted Young's modulus.

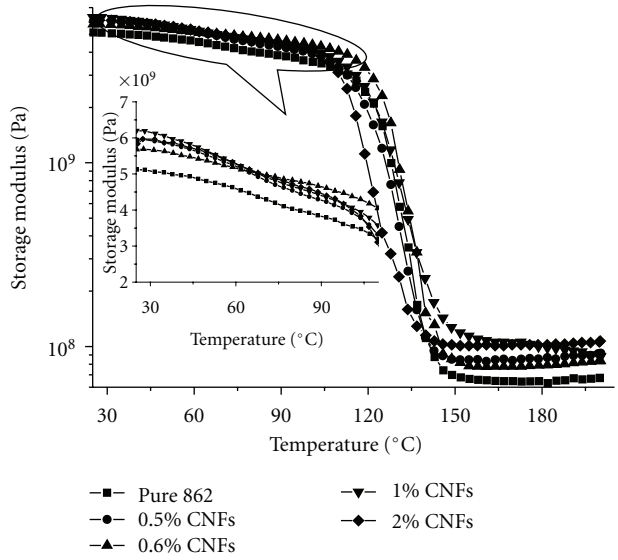

Figure 4: Storage modulus of the pure epoxy and CNF/epoxy nanocomposites.

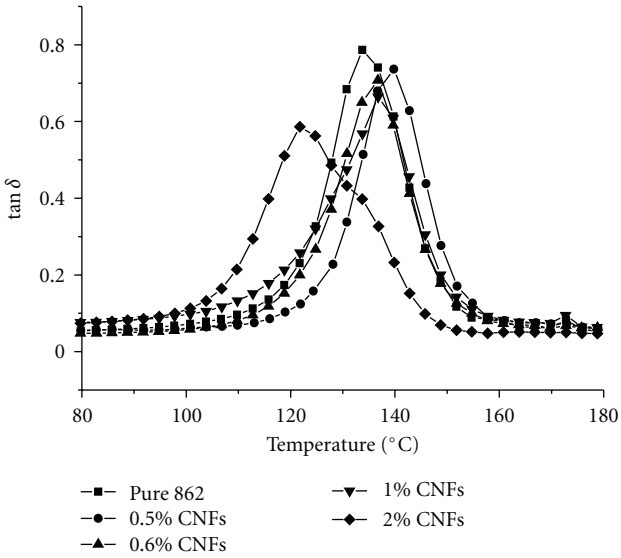

Figure 5: Loss factor of the pure epoxy and CNF/epoxy nanocomposites.

epoxy matrix. There is a hump on the loss factor curve, which further confirms the non-uniformly distributed CNFs. Figure 1(b) clearly shows the dispersion of CNFs in epoxy: large clusters of CNFs are found, but individual fibers are still present. Since the samples of DMA are randomly chosen from the bulk nanocomposite, it is believed that some samples have more CNF clusters, while other samples have more individually dispersed CNFs for the 2 wt% CNF/epoxy nanocomposite. The mobility of molecular chains around CNF clusters is different from that around individual CNFs. Thus, the average value of the loss factor of this nanocomposite has two blunt peaks, indicating two different molecular mobilities around CNF clusters and individual CNFs. Also, the presence of CNF clusters may inhibit the curing of epoxy, thereby decreasing the crosslink density, so that T_g decreases.

The modified Halpin-Tsai equation is also used to fit the experimental data of the storage modulus both below and above T_g. The results are shown in Figure 6. The fitting to the storage modulus is still good for temperatures both below and above T_g. The constants a and b tend to affect the shape of each predicted curve although they do not have clear physical meaning. Figure 6 shows that a and b seem to be higher for high temperatures than those for low temperatures. Also, it is worth pointing out that the deviation of the storage modulus between the samples with the same content of CNFs is relatively large. With the difficulties involved in achieving a uniformly distributed CNF/epoxy nanocomposite, the dispersion of the CNFs is a likely source of error.

3.3. Electrical Properties. Figure 7 shows the electrical conductivity of the pure epoxy and the CNF/epoxy nanocomposites changing with frequency. Conductivity of the pure

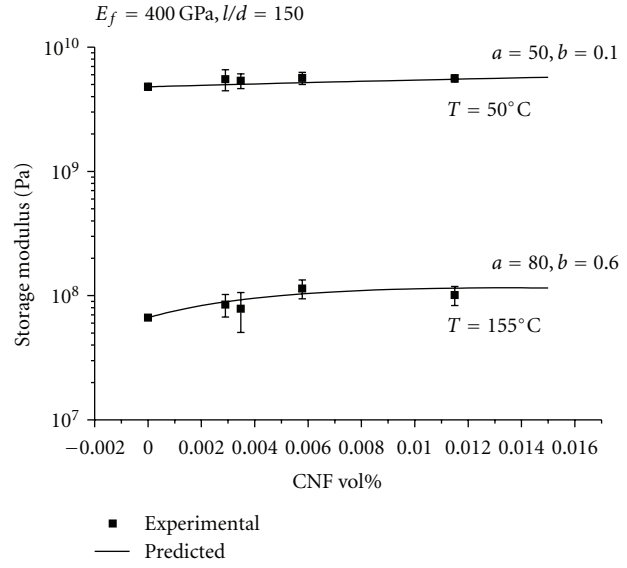

Figure 6: Storage modulus predicted using the modified Halpin-Tsai equation and fitted to the experimental data.

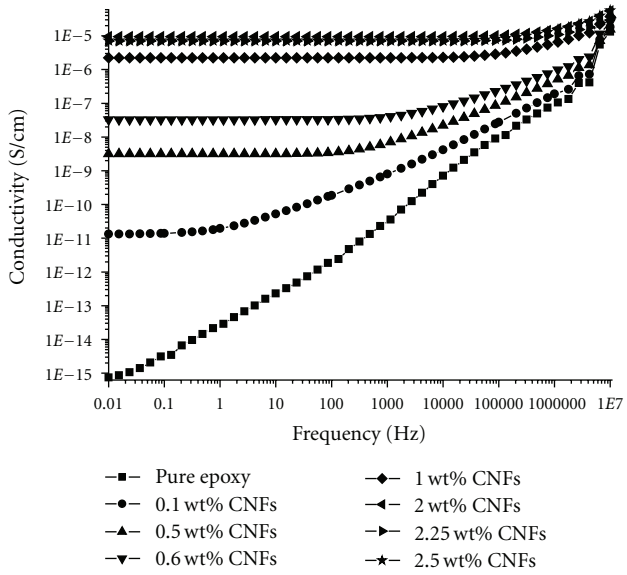

Figure 7: Conductivity of the epoxy nanocomposites with various volume fractions of CNFs as a function of frequency.

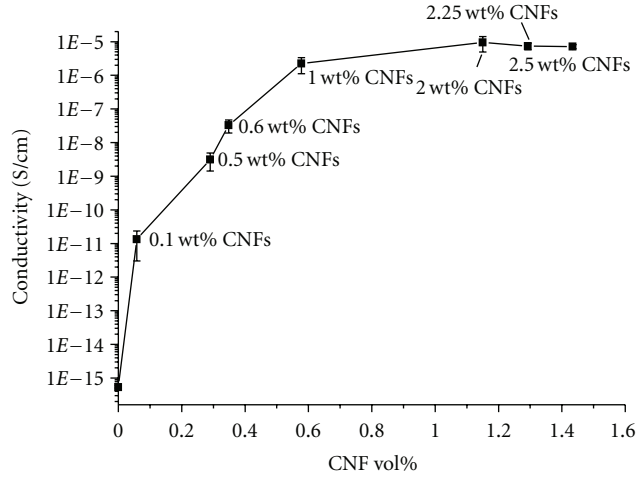

Figure 8: Conductivity varying with the CNF volume fraction.

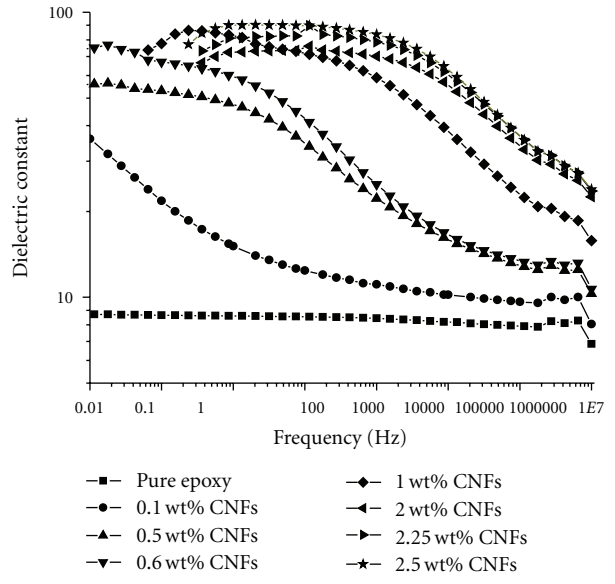

Figure 9: Dielectric constant of the epoxy nanocomposites with various volume fractions of CNFs as a function of frequency.

epoxy is seen to increase almost linearly with increasing frequency, indicating a behavior of a non-conductive material. For the CNF/epoxy nan-ocomposites, the conductivity is independent of frequency at low frequencies but increases with the frequency after critical value is surpassed. The critical frequency at which the conductivity begins to rise increases with the CNF volume fraction. The frequency dependence of the electrical conductivity of the nanocomposites results from the electrons in finite-size clusters with fractal nature that can be scanned at frequencies higher than the critical frequency [10].

The direct-current (DC) conductivities are obtained by extrapolating the conductivity curves of the alternate-current (AC) data. The conductivity is plotted versus the CNF volume fraction (p), as shown in Figure 8. The conductivity increases by four orders of magnitude with the addition of 0.1 wt% (0.058 vol%) CNFs due to the tunneling conduction between CNFs. The value of the CNF volume fraction at which tunneling occurs is called the percolation threshold (p_c). According to percolation theory, the direct-current electrical conductivity σ (at $p > p_c$) of a percolating system should exhibit a power-law dependence: $\sigma \propto (p - p_c)^t$. A best fit to the experimental data reveals that the percolation threshold is 0.057 vol% with the exponent $t = 1.83$. The exponent t is in the range of 1.6 to 2.0, which has been typically used in percolation theory [26–29]. The conductivity increases by ten orders of magnitude for nanocomposites

with CNF volume fractions higher than 1 wt% (0.578 vol%) and then plateaus. This is because CNFs come into contact with each other and form conductive pathways throughout the composites at high CNF volume fractions.

The dielectric constant of the nanocomposites with various volume fractions of CNFs was measured as a function of frequency (Figure 9). The addition of CNFs greatly increases the dielectric constant, and the dielectric constant increases with increasing amount of CNF volume fraction at a given frequency. The dielectric constant of the pure epoxy is independent of frequency, which is the typical behavior of a capacitor. Once CNFs have been added, the dielectric constant of the nanocomposite decreases with frequency. The frequency dependence of dielectric constant results from two effects: one is the polarization effect between clusters inside the solution, and the other is anomalous diffusion within each cluster [30]. At higher frequencies, it is hard for either the polarization or the diffusion to occur because the electrical field changes so fast that they are not able to follow the field variation.

4. Conclusion

CNF/epoxy nanocomposites with various contents of CNFs are processed and studied. Static and dynamic mechanical testing and AC electrical measurements are conducted to investigate the effects of CNFs on the effective properties of the CNF/epoxy nanocomposites. The nanocomposite with 1 wt% CNFs exhibits good dispersion and has the highest tensile strength. The tensile strength decreases with further increase in the CNF content due to agglomeration of CNFs. The maximum storage modulus is also observed in the nanocomposite with 1 wt% CNFs, which is about 18% and 70% higher than that of the pure epoxy below and above the glass transition temperature, respectively. The predicted values of the Young's modulus and storage modulus using a modified Halpin-Tsai equation that accounts for the effect of the CNF agglomeration compares fairly well with those obtained experimentally.

The AC electrical behavior of the CNF/epoxy nanocomposites exhibits a typical insulator-conductor transition. The conductivity increases by four orders of magnitude with the addition of 0.1 wt% (0.058 vol%) CNFs, and by ten orders of magnitude for nanocomposites with CNF volume fractions higher than 1 wt% (0.578 vol%). The measured values of the conductivity of the nanocomposites conform to percolation theory and show a low percolation threshold at 0.057 vol%.

Acknowledgments

The research reported here was conducted in the Electroactive Materials Characterization Laboratory at Texas A&M University. Z. Ounaies acknowledges financial support from NSF (Grant no. CMMI 0514265) and AFOSR (Grant no. FA9550-06-1-0422). X. L. Gao thanks the U.S Army-Soldier Equipment Program for supporting the effort. L. H. Sun and Z. G. Yang are grateful for the support from China Scholarship Council (no. 20083019) and Shanghai Leading Academic Discipline Project (Project no. B113).

References

[1] G. G. Tibbetts, M. L. Lake, K. L. Strong, and B. P. Rice, "A review of the fabrication and properties of vapor-grown carbon nanofiber/polymer composites," *Composites Science and Technology*, vol. 67, no. 7-8, pp. 1709–1718, 2007.

[2] T. Hashishin, H. Iwanaga, M. Ichihara, and S. R. Mukai, "Core structure of vapor grown carbon fibers and morphology dependence of tensile strength," *Carbon*, vol. 41, no. 2, pp. 343–349, 2003.

[3] P. Cortés, K. Lozano, E. V. Barrera, and J. Bonilla-Rios, "Effects of nanofiber treatments on the properties of vapor-grown carbon fiber reinforced polymer composites," *Journal of Applied Polymer Science*, vol. 89, no. 9, pp. 2527–2534, 2003.

[4] S. Kumar, T. Rath, R. N. Mahaling et al., "Study on mechanical, morphological and electrical properties of carbon nanofiber/polyetherimide composites," *Materials Science and Engineering B*, vol. 141, no. 1-2, pp. 61–70, 2007.

[5] K. Lafdi, W. Fox, M. Matzek, and E. Yildiz, "Effect of carbon nanofiber heat treatment on physical properties of polymeric nanocomposites—part I," *Journal of Nanomaterials*, vol. 2007, Article ID 52729, 6 pages, 2007.

[6] R. D. Patton, C. U. Pittman Jr., L. Wang, and J. R. Hill, "Vapor grown carbon fiber composites with epoxy and poly(phenylene sulfide) matrices," *Composites Part A*, vol. 30, no. 9, pp. 1081–1091, 1999.

[7] S.-N. Ahn, H.-J. Lee, B.-J. Kim, L.-S. Tan, and J.-B. Baek, "Epoxy/amine-functionalized short-length vapor-grown carbon nanofiber composites," *Journal of Polymer Science, Part A*, vol. 46, no. 22, pp. 7473–7482, 2008.

[8] K. Lozano and E. V. Barrera, "Nanofiber-reinforced thermoplastic composites. I. Thermoanalytical and mechanical analyses," *Journal of Applied Polymer Science*, vol. 79, no. 1, pp. 125–133, 2001.

[9] Y.-K. Choi, K.-I. Sugimoto, S.-M. Song, Y. Gotoh, Y. Ohkoshi, and M. Endo, "Mechanical and physical properties of epoxy composites reinforced by vapor grown carbon nanofibers," *Carbon*, vol. 43, no. 10, pp. 2199–2208, 2005.

[10] A. Allaoui, S. V. Hoa, and M. D. Pugh, "The electronic transport properties and microstructure of carbon nanofiber/epoxy composites," *Composites Science and Technology*, vol. 68, no. 2, pp. 410–416, 2008.

[11] J. Sandler, P. Werner, M. S. P. Shaffer, V. Demchuk, V. Altstädt, and A. H. Windle, "Carbon-nanofibre-reinforced poly(ether ether ketone) composites," *Composites Part A*, vol. 33, no. 8, pp. 1033–1039, 2002.

[12] H. Ma, J. Zeng, M. L. Realff, S. Kumar, and D. A. Schiraldi, "Processing, structure, and properties of fibers from polyester/carbon nanofiber composites," *Composites Science and Technology*, vol. 63, no. 11, pp. 1617–1628, 2003.

[13] Y. K. Choi, K. I. Sugimoto, S. M. Song, and M. Endo, "Mechanical and thermal properties of vapor-grown carbon nanofiber and polycarbonate composite sheets," *Materials Letters*, vol. 59, no. 27, pp. 3514–3520, 2005.

[14] Y. Zhou, F. Pervin, and S. Jeelani, "Effect vapor grown carbon nanofiber on thermal and mechanical properties of epoxy," *Journal of Materials Science*, vol. 42, no. 17, pp. 7544–7553, 2007.

[15] L. R. Xu, V. Bhamidipati, W.-H. Zhong et al., "Mechanical property characterization of a polymeric nanocomposite reinforced by graphitic nanofibers with reactive linkers," *Journal of Composite Materials*, vol. 38, no. 18, pp. 1563–1582, 2004.

[16] Y. Bin, M. Mine, A. Koganemaru, X. Jiang, and M. Matsuo, "Morphology and mechanical and electrical properties of oriented PVA-VGCF and PVA-MWNT composites," *Polymer*, vol. 47, no. 4, pp. 1308–1317, 2006.

[17] G. D. Liang and S. C. Tjong, "Electrical properties of percolative polystyrene/carbon nanofiber composites," *IEEE Transactions on Dielectrics and Electrical Insulation*, vol. 15, no. 1, pp. 214–220, 2008.

[18] T. Natsuki, Q.-Q. Ni, and S.-H. Wu, "Temperature dependence of electrical resistivity in carbon nanofiber/unsaturated polyester nanocomposites," *Polymer Engineering and Science*, vol. 48, no. 7, pp. 1345–1350, 2008.

[19] R. J. Kuriger, M. K. Alam, D. P. Anderson, and R. L. Jacobsen, "Processing and characterization of aligned vapor grown carbon fiber reinforced polypropylene," *Composites Part A*, vol. 33, no. 1, pp. 53–62, 2002.

[20] J. C. Halpin and J. L. Kardos, "The Halpin-Tsai equations: a review," *Polymer Engineering and Science*, vol. 16, no. 5, pp. 344–352, 1976.

[21] C. L. Tucker III and E. Liang, "Stiffness predictions for unidirectional short-fiber composites: review and evaluation," *Composites Science and Technology*, vol. 59, no. 5, pp. 655–671, 1999.

[22] M.-K. Yeh, N.-H. Tai, and J.-H. Liu, "Mechanical behavior of phenolic-based composites reinforced with multi-walled carbon nanotubes," *Carbon*, vol. 44, no. 1, pp. 1–9, 2006.

[23] M. Van Es, F. Xiqiao, J. Van Turhout, and E. van der Giessen, "Comparing polymer-clay nanocomposites with conventional composites using composite modeling," in *Speciality Polymer Additives: Principles and Applications*, S. Al-Malaika, A. Golovoy, and C. A. Wilkie, Eds., vol. 484, chapter 21, Blackwell Science, Malden, Mass, USA, 2001.

[24] H. P. Menard, *Dynamic Mechanical Analysis, A Practical Introduction*, CRC Press, Taylor & Francis, Boca Raton, Fla, USA, 2008.

[25] Y. Pan, Y. Xu, L. An et al., "Hybrid network structure and mechanical properties of rodlike silicate/cyanate ester nanocomposites," *Macromolecules*, vol. 41, no. 23, pp. 9245–9258, 2008.

[26] D. Stauffer and A. Aharony, *An Introduction to Percolation Theory*, CRC Press, Taylor & Francis, Boca Raton, Fla, USA, 1994.

[27] Z. Ounaies, C. Park, K. E. Wise, E. J. Siochi, and J. S. Harrison, "Electrical properties of single wall carbon nanotube reinforced polyimide composites," *Composites Science and Technology*, vol. 63, no. 11, pp. 1637–1646, 2003.

[28] H. M. Ma and X.-L. Gao, "A three-dimensional Monte Carlo model for electrically conductive polymer matrix composites filled with curved fibers," *Polymer*, vol. 49, no. 19, pp. 4230–4238, 2008.

[29] K. Li, X. L. Gao, J. C. Fielding, and T. B. Tolle, "Modeling of electrical conductivity of nickel nanostrand filled polymer matrix composites," *Journal of Computational and Theoretical Nanoscience*, vol. 6, no. 3, pp. 494–504, 2009.

[30] Y. Song, T. W. Noh, S.-I. Lee, and J. R. Gaines, "Experimental study of the three-dimensional ac conductivity and dielectric constant of a conductor-insulator composite near the percolation threshold," *Physical Review B*, vol. 33, no. 2, pp. 904–908, 1986.